

# Precise determination of stellar parameters of the ZZ Ceti and DAZ white dwarf GD 133 through asteroseismology

J.-N. Fu<sup>1</sup>\*, G. Vauclair<sup>2,3</sup> J. Su<sup>4,5</sup> L. Fox Machado<sup>6</sup> F. Colas<sup>7</sup> S.-L. Kim<sup>8</sup>  
 T. Q. Cang<sup>1,2,3</sup> C. Li<sup>1,9</sup> H. B. Niu<sup>1,10</sup> H. F. Xue<sup>1</sup> Y. Li<sup>4,5</sup> X.-J. Jiang<sup>9</sup>  
 R. Michel<sup>6</sup> M. Alvarez<sup>6</sup> N. Dolez<sup>2,3</sup> L. Ma<sup>10</sup> A. Esamdin<sup>10</sup> and J. Z. Liu<sup>10</sup>

<sup>1</sup> Department of Astronomy, Beijing Normal University, 100875 Beijing, China

<sup>2</sup> Université de Toulouse; UPS-OMP; IRAP; Toulouse, France

<sup>3</sup> CNRS; IRAP; 14 av. Edouard Belin, F-31400 Toulouse, France

<sup>4</sup> Yunnan Observatories, Chinese Academy of Sciences, P.O. Box 110, Kunming 650216, China

<sup>5</sup> Key Laboratory for the Structure and Evolution of Celestial Objects, Chinese Academy of Sciences, P.O. Box 110, Kunming 650216, China

<sup>6</sup> Instituto de Astronomía, Observatorio Astronómico Nacional San Pedro Mártir, Universidad Nacional Autónoma de México, 22860 Ensenada, Baja California, México

<sup>7</sup> IMCCE, Observatoire de Paris, UMR 8028 CNRS, F-75014 Paris, France

<sup>8</sup> Korea Astronomy and Space Science Institute, Daejeon 34055, Korea

<sup>9</sup> National Astronomical Observatories, Chinese Academy of Sciences, 20A Datun Road, Chaoyang District, 100012 Beijing, China

<sup>10</sup> Xinjiang Astronomical Observatory, Chinese Academy of Sciences, Urumqi 830011, China

Accepted XXX. Received YYY; in original form ZZZ

## ABSTRACT

An increasing number of white dwarf stars show atmospheric chemical composition polluted by heavy elements accreted from debris disk material. The existence of such debris disks strongly suggests the presence of one or more planet(s) whose gravitational interaction with rocky planetesimals is responsible for their disruption by tidal effect. The ZZ Ceti pulsator and polluted DAZ white dwarf GD 133 is a good candidate for searching for such a potential planet. We started in 2011 a photometric follow-up of its pulsations. As a result of this work in progress, we used the data gathered from 2011 to 2015 to make an asteroseismological analysis of GD 133, providing the star parameters from a best fit model with  $M/M_{\odot} = 0.630 \pm 0.002$ ,  $T_{\text{eff}} = 12400 \text{ K} \pm 70\text{K}$ ,  $\log(M_{\text{He}}/M) = -2.00 \pm 0.02$ ,  $\log(M_{\text{H}}/M) = -4.50 \pm 0.02$  and determining a rotation period of  $\approx 7$  days.

**Key words:** stars:evolution – stars:white dwarfs – stars:oscillations – stars:individual:GD 133

## 1 INTRODUCTION

An increasing number of white dwarf stars show atmospheric chemical composition polluted by heavy elements accreted from a debris disk. The formation of the debris disk by the tidal disruption of rocky planetesimals suggests that one, or more, still undetected planet(s) may be orbiting the white dwarfs. Their gravitational interaction with the planetesimals may induce the orbital perturbations leading to the planetesimals disruption once they get close to the white dwarf tidal radius. So looking for the signature of such a planet seems justified. We have undertaken this search by starting a long-term follow-up of the ZZ Ceti pulsator and polluted white dwarf GD 133, to look for a periodic variation

of the observed pulse arrival time of the oscillations. On the other hand, carrying-out observation campaigns for the ZZ Ceti pulsators helps also to understand the properties of the oscillations of the target stars and precisely determine stellar parameters through asteroseismology, which are the preconditions of the search for planets. As a preliminary result of this work, we provide in the present paper an asteroseismological analysis of GD 133, which helps to determine the stellar parameters precisely.

### 1.1 GD133 as a ZZ CETI

GD 133 has long been considered as a non-variable DA white dwarf close to the blue edge of the ZZ Ceti instability strip. It has been observed by various teams in an effort to determine precisely the location of the ZZ Ceti in-

\* E-mail: jnfu@bnu.edu.cn

stability strip blue edge. It was on our target list during an observing run in 1986 at the 1.93 m telescope of the Haute-Provence Observatory. We obtained two short runs on November 29th and December 1st. A peak was present in the Fourier-Transform at  $8138 \mu\text{Hz}$  (period  $\approx 123$  s) with an amplitude of 4 mma. However, with a S/N ratio of only  $2.4 \sigma$  this peak was considered as insignificant and this result remained unpublished. Later Kepler et al. (1995) put a 2.7 mma upper limit on the pulsation in GD 133. It was until GD 133 could be observed with the VLT-ULTRACAM that its pulsations were unambiguously detected by Silvotti et al. (2006). The star showed three small amplitude pulsations at 120.4 s, 115.9 s and 146.9 s with amplitudes of 4.6 mma, 1.5 mma and 1.1 mma, respectively. The analysis of the archival Hubble Space Telescope data from the Cosmic Origins Spectrograph reveals the same 3 periods with larger amplitudes in the UV (Sandhaus et al. 2016). In addition a long period variability with a 5.2 hr period is present in these data. With an effective temperature of  $12600 \text{ K} \pm 192 \text{ K}$  (Gianninas, Bergeron & Ruiz 2011), GD 133 should be among the hottest ZZ Ceti pulsators defining the blue edge of the instability strip.

## 1.2 GD133 as a DAZ

GD 133 was reclassified as a DAZ after the discovery of Ca lines in its spectrum by Koester et al. (2005), who derived its atmospheric parameters as  $T_{\text{eff}} = 12200 \text{ K}$ ,  $\log(g) = 7.9$  and an abundance  $[\text{Ca}/\text{H}] = -7.3$ . A number of subsequent analyses have redetermined the atmospheric parameters of GD 133, i.e. Lajoie & Bergeron (2007), Koester et al. (2009), Farihi et al. (2010), Kawka et al. (2011), Gianninas, Bergeron & Ruiz (2011). The most recent work by Xu et al. (2014) revises the estimated Ca abundance as  $[\text{Ca}/\text{H}] = -7.21 \pm 0.13$ , derives abundances for the additional heavy elements O, Mg and Si and updates the atmospheric parameters as  $T_{\text{eff}} = 12600 \text{ K} \pm 200 \text{ K}$ , in agreement with the value derived by Gianninas, Bergeron & Ruiz (2011), and  $\log(g) = 8.10 \pm 0.10$ , from which they derived a mass of  $M/M_{\odot} = 0.66$ .

The heavy elements observed in the atmosphere of GD 133 originate from matter accreted from the debris disk discovered by Jura, Farihi & Zuckerman (2007) (see also Jura, Farihi & Zuckerman 2009; Farihi, Jura & Zuckerman 2009). Their relative abundances are quite similar to the Earth bulk composition (Xu et al. 2014). Once accreted on the white dwarf, they can not remain at the surface. They are rapidly mixed in the convection zone and further deeper in the interior by the fingering convection induced by the inverse  $\mu$  gradient resulting from the accretion (Deal et al. 2013; Vauclair et al. 2015; Wachlin et al. 2017). Their presence in the atmosphere proves that the accretion of material from the debris disk is going on.

## 1.3 Is there a planet orbiting GD133?

The existence of debris disks around white dwarfs is explained by the disruption of rocky planetesimals by tidal effect as soon as their orbit enters the tidal radius of the white dwarfs (Debes & Sigurdsson 2002; Jura 2003, 2008). These planetesimals are the remnants of the pristine planetary system. They have survived the whole central star evolution

through the final white dwarf stage. That such planetesimals disintegration occurs is now an observational evidence after the recent discovery of the planetesimal fragments, including gas components, transiting the white dwarf WD 1145+017 (Vanderburg et al. 2015; Gänsicke et al. 2016; Xu et al. 2016; Rappaport et al. 2016; Croll et al. 2017).

Such planetesimals have to come close to, or cross through, the tidal radius of the white dwarf for being subsequently disintegrated. To achieve this condition, their presumably original circular orbits must be perturbed by gravitational interactions with massive(s) planet(s), of either Jovian or Neptunian sizes, to evolve toward elliptical orbits of large eccentricity so as to pass close enough to the white dwarf tidal radius. A number of scenarios of planetary system evolution through the giant and asymptotic giant branches have demonstrated that such massive planets may survive these phases of the star evolution and be able to perturb the planetesimal orbits to large eccentricity (e.g. Debes & Sigurdsson 2002; Bonsor, Mustill & Wyatt 2011; Debes, Walsh & Stark 2012; Mustill et al. 2013; Veras et al. 2011, 2013, 2014; Veras, Jacobson & Gänsicke 2014; Veras, Eggl & Gänsicke 2015a,b; Veras et al. 2015; Veras 2016; Veras et al. 2016; Frewen & Hansen 2014).

Any potential planet(s) orbiting GD 133 could be detected through a periodic variation of the observed pulse arrival time of the oscillations induced by the time delay due to the orbital motion of the white dwarf around the barycenter of the system. But at the present time no planet has yet been discovered orbiting around white dwarfs by using this technique (Winget et al. 2003; Mullally et al. 2008; Mukadam et al. 2013; Winget et al. 2015).

As an example, a Jovian mass planet orbiting a  $M_* = 0.6 M_{\odot}$  white dwarf on a circular orbit with a 1 AU semi-major axis would imply a 0.8 s change in the arrival time  $\tau$ , on an orbital period of  $\approx 1.2$  years. For a Neptunian mass planet orbiting at 7 AU  $\tau$  would be  $\approx 0.3$  s on a 24 years orbital period. Such orbital motions could be detectable through the change of the observed pulsation periods and/or in a O-C diagram. This detectability increases with both the distance of the planet to its star  $a_p$  and the planet mass  $m_p$  according to Mullally et al. (2008):

$$\tau = a_p m_p \sin i / M_* c,$$

where  $i$  is the inclination angle of the planet orbital plane on the line of sight.

We have selected GD 133 to study because to make such a measurement, one needs to choose a ZZ Ceti star close to the blue edge of the instability strip where they show only a few periods, stable in both their periods and amplitudes. The cool ZZ Ceti stars are unsuitable because of the growing nonlinear interactions of the pulsations with convection. Such interactions induce complex power spectrum with frequency combinations and amplitude variations which makes difficult a precise measurement of the periods. One also needs to avoid large amplitude ZZ Ceti stars because of the nonlinear effects induced by the large amplitudes. GD 133 as a low amplitude ZZ Ceti pulsator close to the blue edge of the instability strip and as a polluted DAZ accreting heavy material from a debris disk detected through its IR excess is an ideal target to attempt the detection of a potential orbiting planet. In addition, the disk is

**Table 1.** Journal of observations: 2011

Run_Name	Telescope	Date (UT)	Start_Time (UTC)	Run_Length (frames)
sp0302	SPM 1.5-m	02 March	04:37:02	858
sp0304	SPM 1.5-m	04 March	04:29:52	800
lj0304	LiJiang 2.4-m	04 March	15:33:39	55
2011034	PdM 1-m	04 March	20:29:58	963
sp0305	SPM 1.5-m	05 March	04:36:47	800
lj0305	LiJiang 2.4-m	05 March	15:38:15	181
20110305	PdM 1-m	05 March	20:24:10	985
sp0306	SPM 1.5-m	06 March	04:21:59	856
lj0306	LiJiang 2.4-m	06 March	14:08:46	780
20110306	PdM 1-m	06 March	20:33:24	951
lj0307	LiJiang 2.4-m	07 March	13:53:35	728
20110307	PdM 1-m	07 March	20:13:06	1000
sp0308	SPM 1.5-m	08 March	06:22:43	599
lj0308	LiJiang 2.4-m	08 March	13:41:33	806
20110308	PdM 1-m	08 March	19:44:53	836
sp0309	SPM 1.5-m	09 March	04:16:06	881

seen almost edge-on, according to the disk best-fit model described by [Jura, Farihi & Zuckerman \(2009\)](#) who derived an inclination angle of  $\approx 79$  deg. Assuming that the perturbing planet lies in the same plane than the disk makes the case most favorable for a detection. We have undertaken a long term photometric follow-up of the GD 133 pulsations which started in 2011. In the present paper, we use the data gathered up to now to determine the star parameters through asteroseismology.

The paper is organized as follows. Section 2 describes the observations obtained since 2011. Data analysis is presented in section 3. In section 4 we describe the method for determining the best-fit model and discuss the results. A summary and the conclusions are given in section 5.

## 2 OBSERVATIONS

We observed GD 133 during a first multisite campaign from March 2 to March 9, 2011. The campaign included three observing sites: San Pedro Mártir (SPM) observatory (Mexico), with the 1.5 m telescope; LiJiang observatory (Yunnan, China), with the 2.4 m telescope and Pic-du-Midi (PdM) observatory (France), with the 1 m telescope. Table 1 gives the journal of the observations. The cycle time was 35 s at SPM and 30 s for both LiJiang and PdM. We obtained 106 hours of photometric data for a campaign total duration of 174.6 hours, i.e. a 60.7% duty cycle.

A second campaign was organized in 2013 from two sites. But the observations were not obtained simultaneously from the two sites. The 1.8 m telescope of the Bohyunsan Optical Astronomical Observatory (BOAO, Korea) made observations between March 11 and March 16, 2013. The observations were continued with the 84 cm telescope

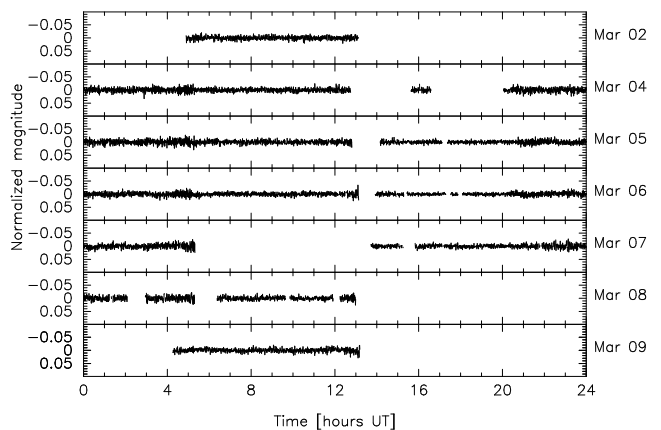


**Figure 1.** Normalized light curve of GD 133 during the 2011 campaign. The normalized magnitude, indicated on the left side, is plotted as a function of time (UT). Each panel covers a 24 h period; the date is indicated on the right side.

**Table 2.** Journal of observations: 2013

Run_Name	Telescope	Date (UT)	Start_Time (UTC)	Run_Length (frames)
boao0311	BOAO 1.8-m	11 March	12:32:59	1196
boao0314	BOAO 1.8-m	14 March	11:37:19	833
boao0315	BOAO 1.8-m	15 March	11:28:57	1242
boao0316	BOAO 1.8-m	16 March	11:37:11	1353
20130323	SPM 84-cm	23 March	04:44:38	664
20130324	SPM 84-cm	24 March	03:27:42	1050
20130325	SPM 84-cm	25 March	03:02:25	1139
20130326	SPM 84-cm	26 March	03:23:14	722
20130328	SPM 84-cm	28 March	07:45:40	332
20130329	SPM 84-cm	29 March	03:20:44	910
20130330	SPM 84-cm	30 March	03:40:42	588
20130331	SPM 84-cm	31 March	03:37:40	739

of the San Pedro Mártir (SPM) observatory (Mexico). Table 2 gives the journal of the 2013 observations. The observing cycle time were 35 s at BOAO and 39 s at SPM. Taking separately the two contributions to the campaign we obtained 26 h of photometric data during the 126.7 h of the BOAO part of the campaign, i.e. a 20.5% duty cycle, and 37 h of photometric data during the 313 h of the SPM part, i.e. a 11.8% duty cycle. For the whole campaign, including the gap between the BOAO and the SPM observations, we obtained a duty cycle of 14%.

In 2014, a third campaign was organized, including two sites in China: the Xinglong Station (XL) of the National Astronomical Observatories of China (NAOC), with the 2.16 m and the 85 cm telescopes, and the Nanshan observatory (Xinjiang, China), with the 1 m telescope. Data were obtained from February 27 to March 6, 2014. Table 3 gives the journal of the 2014 campaign. The observing cycle was 29 s on the XL 2.16 m and 28 s on the 85 cm. On the Nanshan

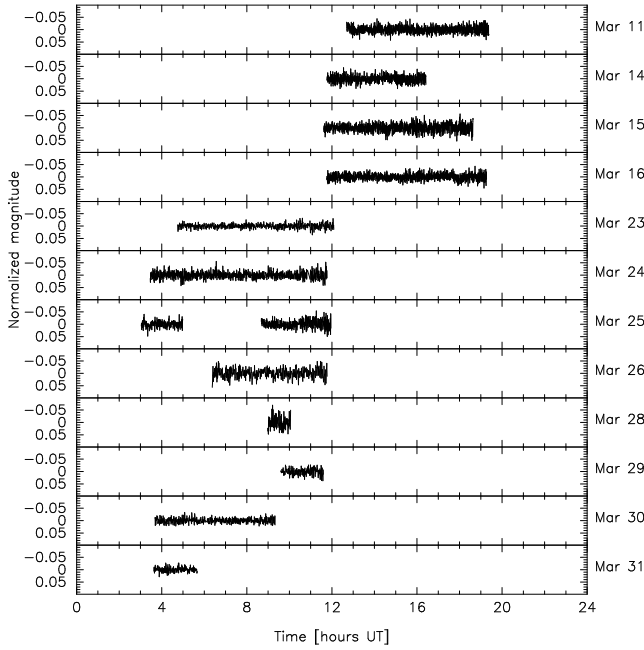


Figure 2. Same as Fig.1 for the 2013 campaign.

Table 3. Journal of observations: 2014

Run_Name	Telescope	Date (UT)	Start_Time (UTC)	Run_Length (frames)
xl0227	Xinglong 2.16-m	27 February	13:43:03	642
xl0301	Xinglong 85-cm	01 March	13:44:48	848
ns0301	Nanshan 1.0-m	01 March	15:53:05	478
xl0302	Xinglong 85-cm	02 March	13:28:39	899
ns0302	Nanshan 1.0-m	02 March	15:31:42	966
ns0303	Nanshan 1.0-m	03 March	17:00:32	781
xl0304	Xinglong 85-cm	04 March	13:52:07	758
ns0304	Nanshan 1.0-m	04 March	15:43:01	910
xl0305	Xinglong 85-cm	05 March	13:48:29	705
xl0306	Xinglong 85-cm	06 March	13:53:31	775

1 m the cycle time was adapted to the observing conditions: it was 44 s on March 1, 21 s on March 2, 24 s on March 3 and 20 s on March 4. We obtained 53.2 h of photometric data during the 175 h of the campaign, i.e. a duty cycle of 30.4%.

In 2015, the multisite campaign was organized from March 13 to 23. We used the 2.16 m telescope in Xinglong and the 1 m telescope in Nanshan (China), the 1 m telescope in Pic-du-Midi Observatory (France) and the 84 cm telescope at San Pedro Mártir (Mexico). Table 4 gives the journal of the 2015 observations. The observing cycles were 42 s on the Xinglong 2.16 m telescope, 22 s on the 1 m telescope at Pic du Midi, 42 s on the 84 cm at SPM. On the 1 m telescope of Nanshan, the observing cycle was adapted according to the observing conditions but is 30 s in aver-

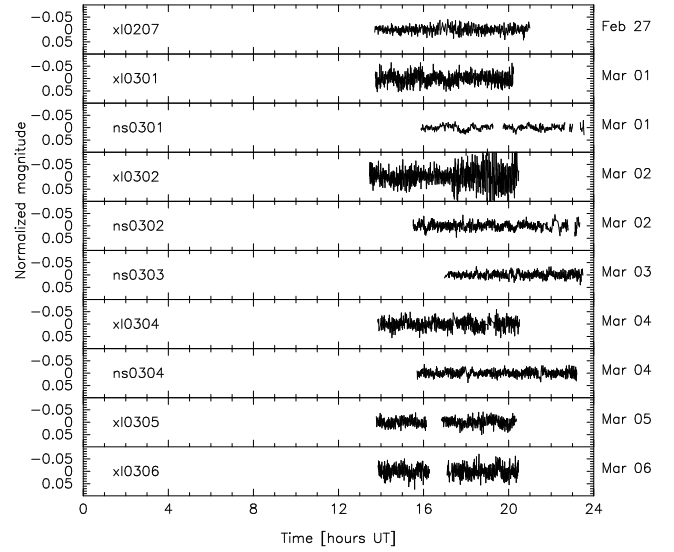


Figure 3. Same as Fig.1 for the 2014 campaign.

Table 4. Journal of observations: 2015

Run_Name	Telescope	Date (UT)	Start_Time (UTC)	Run_Length (frames)
ns0313	Nanshan 1-m	13 March	14:40:56	853
ns0314	Nanshan 1-m	14 March	20:12:29	153
ns0315	Nanshan 1-m	15 March	14:49:22	438
ns0316	Nanshan 1-m	16 March	16:39:46	397
spm317	SPM 84-cm	17 March	05:14:38	369
ns0317	Nanshan 1-m	17 March	16:01:11	688
xl0318	Xinglong 2.16-m	18 March	12:29:04	633
xl0319	Xinglong 2.16-m	19 March	12:28:54	617
pdm319	PdM 1-m	19 March	22:49:00	766
xl0320	Xinglong 2.16-m	20 March	12:52:28	602
xl0321	Xinglong 2.16-m	21 March	12:23:40	479
xl0322	Xinglong 2.16-m	22 March	12:18:32	646
xl0323	Xinglong 2.16-m	23 March	12:14:55	639

age. We obtain a total of 72.2 h of data on the 245 h of the campaign total duration, i.e. a duty cycle of 29%.

### 3 DATA ANALYSIS

All the data were reduced with the standard IRAF routines. The IRAF AP-PHOT package was used to perform aperture photometry. Different size of apertures were optimized for each night in order to obtain the minimum variance of the light curves of a check star relative to the comparison star. The light curve of GD 133 relative to the comparison star was then obtained for each campaign. A fifth order polynomial was applied to filter the low frequency induced by variations of the atmosphere transparency during the night.

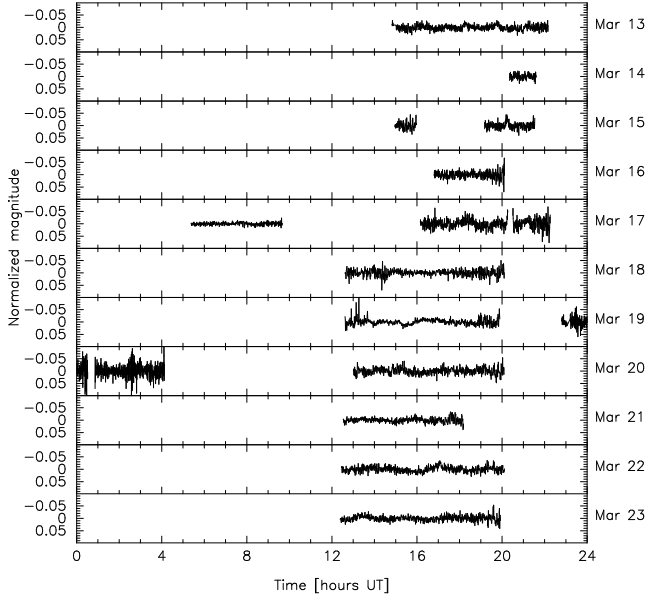


**Figure 4.** Same as Fig.1 for the 2015 campaign.

The normalized light curves for the 2011, 2013, 2014 and 2015 are shown in Figures 1, 2, 3 and 4, respectively.

The normalized light curve of each campaign was analyzed with the PERIOD04 software (Lenz & Breger 2005) to perform Fourier transform (FT). The standard prewhitening procedure was then applied to extract the frequencies, the amplitudes and the phases of the signals from the FT spectrum. Figures 5, 7, 8 and 9 show the Fourier transforms (actually the amplitude spectra) for the 2011, 2013, 2014 and 2015 campaign respectively. Figure 6 illustrates the pre-whitening process in details on the 2011 FT. We extract the signals from the pre-whitening process which have a signal/noise (S/N) ratio larger than 4, following the prescription given by Breger et al. (1993) and Kuschnig et al. (1997). PERIOD04 estimates the internal uncertainties on the frequencies and amplitudes, which are generally underestimated. More realistic uncertainties were derived by using Monte-Carlo simulations as described in Fu et al. (2013). In the case of the 2011 campaign we extracted the 8 signals listed in Table 5. The signals extracted for the 2013, 2014 and 2015 campaigns are listed in the Tables 6, 7 and 8 respectively. All the uncertainties quoted in the Tables are derived from the Monte-Carlo simulations. We note that we never see any linear combinations of frequencies in our data. That is in agreement with what is expected for a low amplitude pulsator close to the blue edge of the ZZ Ceti instability strip.

**Table 5.** Frequencies and amplitudes of GD 133 during the 2011 campaign. The frequencies,  $\nu$ , are given in  $\mu\text{Hz}$  and the amplitudes,  $A$ , in millimagnitude (mmag). The uncertainties are estimated through Monte-Carlo simulations.

$\nu$ ( $\mu\text{Hz}$ )	$\sigma(\nu)$ ( $\mu\text{Hz}$ )	$A$ (mmag)	$\sigma(A)$ (mmag)	$P$ (s)	$\sigma(P)$ (s)
2821.74	0.34	0.47	0.15	354.391	0.042
5106.04	0.31	0.55	0.20	195.846	0.012
6818.48	0.14	1.33	0.51	146.660	0.003
6821.89	0.14	1.24	0.38	146.586	0.003
8308.81	0.16	1.95	0.43	120.354	0.002
8310.28	0.12	2.24	0.58	120.332	0.002
8625.25	0.15	0.72	0.25	115.938	0.002
8628.57	0.15	0.62	0.19	115.894	0.002

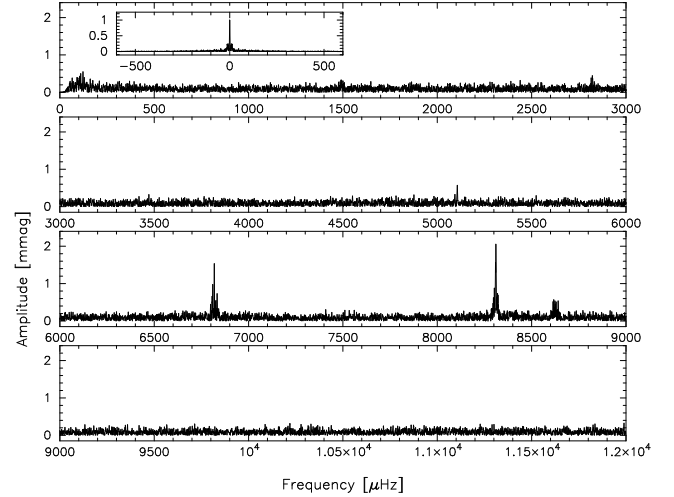


**Figure 5.** Amplitude spectrum of the 2011 light curve. The four panels show the amplitude spectrum in units of milli-magnitude (mmag) as a function of the frequency in  $\mu\text{Hz}$ , in the frequency range 0-12000  $\mu\text{Hz}$ . The corresponding window function is shown on the same scale in the insert.

**Table 6.** Frequencies and amplitudes of GD 133 during the 2013 campaign.

$\nu$ ( $\mu\text{Hz}$ )	$\sigma(\nu)$ ( $\mu\text{Hz}$ )	$A$ (mmag)	$\sigma(A)$ (mmag)	$P$ (s)	$\sigma(P)$ (s)
6817.40	0.02	1.10	0.20	146.6835	0.0004
6821.82	0.04	0.90	0.20	146.5884	0.0008
8308.69	0.02	1.80	0.10	120.3559	0.0003
8310.51	0.02	1.90	0.20	120.3296	0.0003
8623.56	0.04	0.80	0.20	115.9614	0.0005
8628.65	0.04	1.00	0.10	115.8930	0.0005



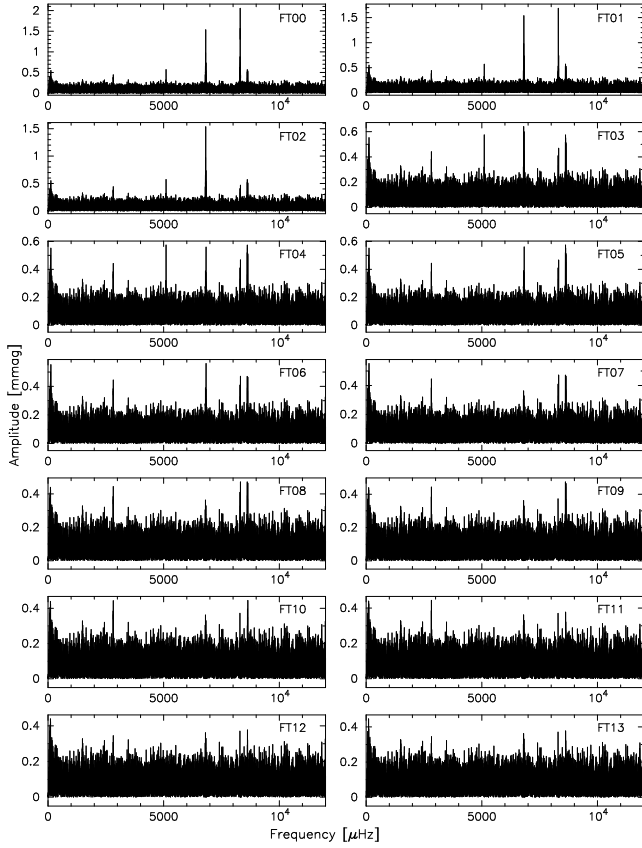


**Figure 6.** Illustration of the prewhitening process on the 2011 amplitude spectrum. The first panel (FT00) is the full amplitude spectrum as shown in Fig.5. Panel FT01 shows the amplitude spectrum after subtraction of the largest amplitude peak at  $8310 \mu\text{Hz}$ . The next panel (FT02) shows the amplitude spectrum after additional subtraction of the next largest amplitude peak at  $8308 \mu\text{Hz}$ , and so on for the subsequent panels. Note that the Y-axis scale is optimized according to the height of the largest peak in each panel.

**Table 7.** Frequencies and amplitudes of GD 133 during the 2014 campaign.

$\nu$ ( $\mu\text{Hz}$ )	$\sigma(\nu)$ ( $\mu\text{Hz}$ )	$A$ (mmag)	$\sigma(A)$ (mmag)	$P$ (s)	$\sigma(P)$ (s)
6819.99	0.28	1.88	0.09	146.6278	0.006
6821.72	0.27	1.61	0.07	146.5906	0.006
8310.16	0.26	3.23	0.15	120.3346	0.004

## 4 MODELLING

### 4.1 Theoretical models

The Modules for Experiments in Stellar Astrophysics (MESA, see Paxton et al. 2011, 2013, 2015, for details) was employed for creating carbon-oxygen white dwarf models. MESA creates a white dwarf model from a zero-age main sequence model, with an initial chemical composition  $X=0.7$ ,  $Y=0.28$  and  $Z=0.02$ . The initial model evolves through

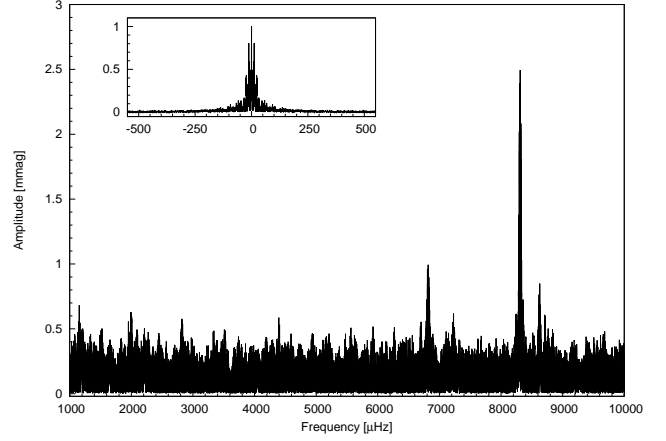


**Figure 7.** Same as Fig.5 for the 2013 light curve. Amplitude spectrum of the 2013 light curve with the frequency range 1000-10000  $\mu\text{Hz}$ .

**Table 8.** Frequencies and amplitudes of GD 133 during the 2015 campaign.

$\nu$ ( $\mu\text{Hz}$ )	$\sigma(\nu)$ ( $\mu\text{Hz}$ )	$A$ (mmag)	$\sigma(A)$ (mmag)	$P$ (s)	$\sigma(P)$ (s)
6818.69	0.09	1.37	0.23	146.655	0.002
6821.51	0.12	1.49	0.27	146.595	0.003
6832.56	0.14	1.16	0.27	146.358	0.003
8308.68	0.06	1.95	0.21	120.356	0.001
8310.30	0.05	2.18	0.21	120.332	0.001

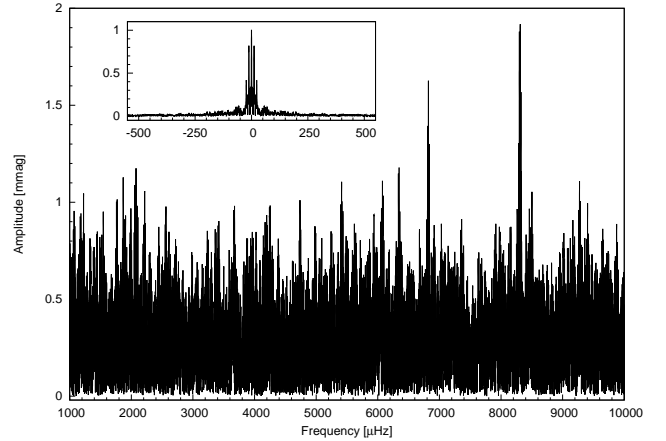


**Figure 8.** Same as Fig. 7 for the 2014 light curve.

main sequence and post main sequence stages with mass loss, until it remains a hot degenerate C-O core with the central temperature  $T_c \sim 10^8$  K. The mass of the initial model is varied from  $0.8$  to  $8 M_\odot$  to get a series of C-O models with different masses. The masses of the C-O models we obtained are distributed from  $0.45$  to  $0.9 M_\odot$ .

In addition, an updated version of the White Dwarf

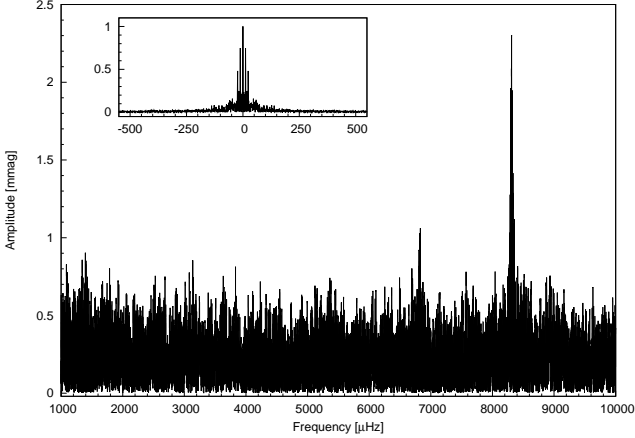


**Figure 9.** Same as Fig. 7 for the 2015 light curve.

Evolution Code (WDEC, Bradley 1993; Montgomery 1998) was used to construct DA white dwarf models by adjusting and relaxing the C-O models prepared by MESA. The masses of the helium and hydrogen layers are adjustable parameters in WDEC. It constructs H/He envelopes of given masses and chemical compositions to make DA white dwarf models. So we can conveniently obtain a model with defined parameters by choosing an initial model of given mass ( $M/M_{\odot}$ ), setting its input parameters ( $M_{\text{He}}/M$  and  $M_{\text{H}}/M$ ) and evolving it to a specified effective temperature ( $T_{\text{eff}}$ ). Repeating the calculation, we can get a series of models with different stellar parameters to form a model grid for the asteroseismology analysis.

In this work, a modified version of WDEC (Su et al. 2014) is adopted. The main modification is to incorporate the treatment of the gravitational settling into the code, which solves diffusion equations using the diffusion velocities and coefficients as given by Thoul, Bahcall & Loeb (1994). Four elements ( $^1\text{H}$ ,  $^4\text{He}$ ,  $^{12}\text{C}$  and  $^{16}\text{O}$ ) are taken into account. All elements are assumed to be fully ionized and electrons are considered as an individual component. With the updates, the models have more physically realistic chemical profiles of the composition transition zones (e.g. H/He, He/C/O) than previous works (for example, Su & Li 2010), where transition zones were approximated by parametric equilibrium profiles.

A pulsation code (Su et al. 2014), which solves the adiabatic oscillation equations to get eigenfrequencies and eigenfunctions, is adopted to calculate the theoretical frequencies of the models.

Taking into account the abundances of the elements determined by Xu et al. (2014), we derive the metallicity of GD 133 to be approximately  $Z = 3.3 \times 10^{-5}$ . In this framework, we consider that the heavy elements are mixed in the whole H outer layers as a consequence of the fingering convection (Deal et al. 2013). We use an equivalent carbon abundance in our models to represent all of other heavy elements.

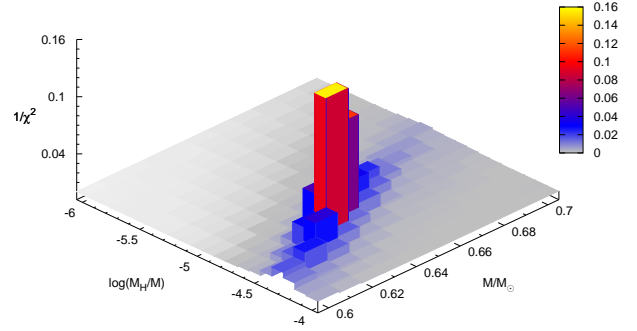


**Figure 10.** 3D  $\chi^2$  distribution of the model grid as a function of  $M/M_{\odot}$  and  $\log(M_{\text{H}}/M)$ . For a better visibility,  $1/\chi^2$  is plotted with the corresponding color scale.

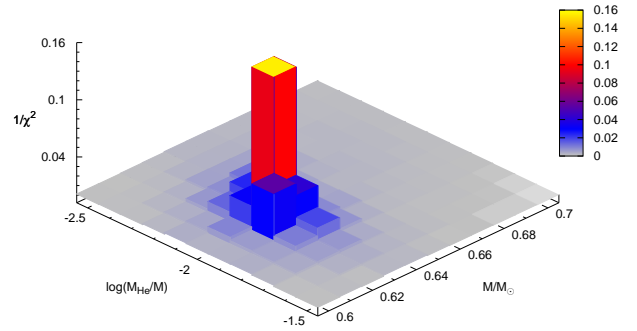


**Figure 11.** Same as figure 10:  $\chi^2$  as a function of  $M/M_{\odot}$  and  $\log(M_{\text{He}}/M)$ .

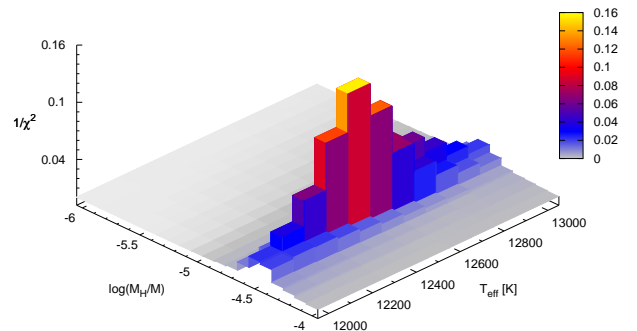


**Figure 12.** Same as figure 10:  $\chi^2$  as a function of  $T_{\text{eff}}$  and  $\log(M_{\text{H}}/M)$ .

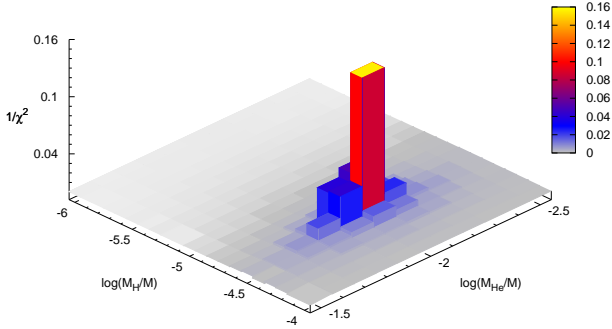


**Figure 13.** Same as figure 10:  $\chi^2$  as a function of  $\log(M_{\text{He}}/M$  and  $\log(M_{\text{H}}/M)$ .

## 4.2 Asteroseismological analysis

The aim of the asteroseismology analysis is to find a best-fitting model by matching the theoretical periods to the observed ones. It helps us to constrain the stellar parameters of GD 133. We used the frequencies derived from the 2011 multisite campaign for which we got the best duty cycle. Five periods at 115.9, 120.3, 146.7, 195.8 and 354.4 s (the corresponding frequencies are 8625.2, 8310.3, 6818.5, 5106.0 and 2821.7  $\mu\text{Hz}$ ) are used to perform asteroseismological analysis. Note that we take the frequencies of the components whose amplitudes are the largest in the corresponding multiplets, i.e. 8625.2, 8310.3, and 6818.5  $\mu\text{Hz}$ . The evaluation of the matching degree for each model is defined as:

$$\chi^2 \equiv \sum_{i=1}^N (P_{\text{ob}}^i - P_{\text{th}}^i)^2, \quad (1)$$

where  $P_{\text{ob}}^i$  are the observed periods,  $P_{\text{th}}^i$  are the theoretical periods calculated with the model and  $N$  is the total number of observed periods. The model with minimum  $\chi^2$  is considered to be the best-fitting model. We only calculate theoretical periods with spherical harmonic degree  $\ell=1$  and  $\ell=2$ . Pulsation modes with higher  $\ell$  values are neglected since the geometrical cancellation makes them hardly to be observed photometrically (see [Castanheira & Kepler 2008](#), and references therein). We perform a so-called blind matching on each observed period. It lets each observed period to match the theoretical periods of either  $\ell=1$  or  $\ell=2$ . Then it selects the theoretical period which is the closest one to the observed period and uses it as the  $i$ -th  $P_{\text{th}}$  to evaluate the  $\chi^2$ . One will note that the two periods 116.0 and 120.3 s are quite close together. The period spacing between them is significantly less than the typical value for low-order g modes. This means these two periods should not be assigned to the same  $\ell$  degree. If the period 116.0 s is  $\ell=1$  mode, the period 120.3 s must be  $\ell=2$ , and vice versa. In addition, we have assumed implicitly that all of observed periods are  $m=0$  modes, since at this stage of analysis we lack enough evidence to determine their  $m$  values. We discuss this point in the next section.

The spectroscopic analysis ([Xu et al. 2014](#)) gives the

atmospheric parameters of GD 133 as  $T_{\text{eff}}=12600 \pm 200$  K and  $\log(g)=8.10 \pm 0.10$ . From  $\log(g)$  and its uncertainty, the estimation of mass is about  $0.65 \pm 0.05 M_{\odot}$ . In order to determine the best-fit model, we computed a grid of models in the 4-D parameter space for  $M/M_{\odot}$ ,  $T_{\text{eff}}$ ,  $\log(M_{\text{He}}/M)$  and  $\log(M_{\text{H}}/M)$ . The range of stellar parameters to explore is set as:

$$\begin{aligned} 0.60 &\leq M/M_{\odot} \leq 0.70, \\ 12000 &\leq T_{\text{eff}} \leq 13000 \text{ K}, \\ -2.5 &\leq \log(M_{\text{He}}/M) \leq -1.5, \\ -10 &\leq \log(M_{\text{H}}/M) \leq -4. \end{aligned}$$

The resolution of the grid is  $\Delta_{M/M_{\odot}}=0.01$ ,  $\Delta_{T_{\text{eff}}}=100$  K,  $\Delta_{\log(M_{\text{He}}/M)}=0.1$  and  $\Delta_{\log(M_{\text{H}}/M)}=0.1$ .

We find out the best-fitting model with a minimum  $\chi^2$  of 6.40. The model parameters of the best-fitting model are  $M/M_{\odot}=0.63$ ,  $T_{\text{eff}}=12400$  K,  $\log(M_{\text{He}}/M)=-2$ ,  $\log(M_{\text{H}}/M)=-4.5$  and the surface gravity derived from the model is  $\log(g)=8.09$ . The distribution of  $\chi^2$  in the 4-D parameter space can be shown as 3D-figures plotting the  $\chi^2$  values in a 2-D plane for two of the parameters with the other two parameters fixed at the values of the best-fit model. We show four of these figures for the  $\chi^2$  distribution as function of  $M/M_{\odot}$  and  $\log(M_{\text{H}}/M)$ ,  $M/M_{\odot}$  and  $\log(M_{\text{He}}/M)$ ,  $T_{\text{eff}}$  and  $\log(M_{\text{H}}/M)$ , and  $\log(M_{\text{He}}/M)$  and  $\log(M_{\text{H}}/M)$  in Fig.10, 11, 12 and 13 respectively.

The uncertainties on the best-fit model parameters are estimated by using the prescription derived by [Zhang, Robinson & Nather \(1986\)](#) which was adopted by [Castanheira & Kepler \(2008\)](#) and [Romero et al. \(2012\)](#). That is:

$$\sigma^2 = d^2 / (S - S_0),$$

where  $\sigma$  is the uncertainty of the parameter,  $d$  is chosen as the step of the parameter within the model grid.  $S_0$  is the  $\chi^2$  of the best-fit model (i.e. the minimum value) and  $S$  is the value of  $\chi^2$  for the model with the prescribed change of the parameter by the amount  $d$ , while keeping all the other parameters fixed. The best-fit model parameters and their uncertainties are:

$$\begin{aligned} M/M_{\odot} &= 0.630 \pm 0.002, \\ T_{\text{eff}} &= 12400 \text{ K} \pm 70 \text{ K}, \\ \log(M_{\text{He}}/M) &= -2.00 \pm 0.02, \\ \log(M_{\text{H}}/M) &= -4.50 \pm 0.02 \end{aligned}$$

The effective temperature and the mass of the best-fit model determined from our asteroseismic analysis are in excellent agreement with the parameters derived from the GAIA precise photometry and parallax measurement:  $T_{\text{eff}}=12259 \text{ K} \pm 68 \text{ K}$  and  $M/M_{\odot}=0.631 \pm 0.005$  ([Gentile Fusillo et al. 2019](#)). The hydrogen mass fraction derived for GD 133 may be compared to the hydrogen mass fractions estimated in some other DAV pulsators. In their analysis of 44 DAVs, [Romero et al. \(2012\)](#) find a range of hydrogen mass fraction  $-9.3 \leq \log(M_{\text{H}}/M) \leq -4$ . In the case of the well studied DAV G 117-B15A, this value is  $-5.9$ . Two other examples of hydrogen mass fraction estimated from asteroseismology of DAVs are for KUV 08368+4026 with  $\log(M_{\text{H}}/M)=-4.0$  ([Li et al. 2015](#)) and HS 0507+0434B with  $\log(M_{\text{H}}/M)=-8.5$  ([Fu et al. 2013](#)).



The theoretical periods of the best-fitting model between 110 and 380 s are listed in Table 9. The five observed periods are listed beside the theoretical periods which they are matched to. The absolute values of difference between  $P_{\text{th}}$  and  $P_{\text{ob}}$  are also listed in the table.

### 4.3 Discussion on the multiplets and on the rotational splitting

The dominant modes observed in GD 133 are the two multiplets around 8310 and 6821  $\mu\text{Hz}$ .

The first one is identified as a  $\ell = 1$  mode. It is a triplet seen as a doublet during each campaign except during the 2014 campaign when only the high frequency component is seen. One can reasonably assume that the rotation axis of the star is perpendicular to the plane of the debris disk, which has an inclination angle of  $\approx 79$  deg on the line of sight according to Jura, Farihi & Zuckerman (2009). In this configuration, the star is seen almost equator-on and only the  $m = -1$  and  $+1$  components of the triplet are visible (Gizon & Solanki 2003). This is in excellent agreement with the fact that one sees only a doublet. The frequency splitting between the two components, averaged on the values measured during the 2011, 2013 and 2015 campaigns, is  $1.64 \pm 0.12 \mu\text{Hz}$ , which corresponds to twice the rotational splitting  $\delta\nu_1 = 0.82 \mu\text{Hz}$ . We use this value to determine the rotation period by using:

$$\omega_{\ell,n,m} = \omega_{\ell,n} + (1 - C_{\ell,n})\Omega,$$

where  $\Omega$  is the rotation frequency.

This mode is identified in the best-fit model as the  $\ell = 1$ ,  $n = 1$  mode. To estimate the rotation period of the star one must compute the  $C_{1,1}$  term since for such low order modes the star is not in the asymptotic regime. As a matter of fact, we find a value of 0.49996. This value is close to the value 0.5 characteristic of the asymptotic regime, suggesting that the mode is a trapped one. We derive a rotation period of  $169 \pm 24\text{h}$  ( $\approx 7.0 \pm 1.0$  days). This is a rather slow rotation compared to other white dwarfs with rotation period derived from asteroseismology.

## 5 SUMMARY AND CONCLUSIONS

The white dwarf GD 133 is a promising candidate to harbor one or more planet(s) as it is surrounded by a debris disk and exhibits an atmospheric composition polluted by heavy elements accreted from the debris disk. Tidal disruption of small rocky bodies, asteroid-like, is considered as the physical process resulting in the formation of such disks. Most scenarii invoke the presence of a larger mass body, of the size of a planet, in order to perturb their orbit to a large enough eccentricity and make them reaching the white dwarf tidal radius where they are disrupted. As GD 133 is also a ZZ Ceti pulsator close to the instability strip blue edge, one may search for the signature of such a potential planet through a periodic variation of the observed pulsation periods induced by the orbital motion. We have undertaken in 2011 a photometric follow-up of GD 133 to search for such a potential signature. In the present paper we describe the data which have been gathered from 2011 to 2015. From the time series analysis we identify five independent pulsation modes, which

**Table 9.** List of theoretical periods ( $P_{\text{th}}$ ) of the best-fitting model between 110 and 380 s. The first column is the spherical harmonic degree  $\ell$  and the second column radial order  $n$ . The five observed periods ( $P_{\text{ob}}$ ) are listed beside the matched theoretical periods in the fourth column and  $|P_{\text{th}} - P_{\text{ob}}|$  are listed in the fifth column.

$\ell$	$n$	$P_{\text{th}}$ (s)	$P_{\text{ob}}$ (s)	$ P_{\text{th}} - P_{\text{ob}} $ (s)
1	1	120.88	120.332	0.55
1	2	196.61	195.846	0.76
1	3	250.43		
1	4	315.75		
1	5	354.85	354.391	0.46
1	6	378.36		
2	2	114.85	115.938	1.09
2	3	144.63	146.660	2.03
2	4	182.66		
2	5	205.30		
2	6	244.61		
2	7	265.04		
2	8	273.75		
2	9	310.27		
2	10	336.53		
2	11	367.38		
2	12	378.67		

are used to make a seismic modelling of the star and derive its main parameters. The parameters of the best-fitting model are  $M/M_{\odot} = 0.630 \pm 0.002$ ,  $T_{\text{eff}} = 12400 \text{ K} \pm 70 \text{ K}$ ,  $\log(M_{\text{He}}/M) = -2.00 \pm 0.02$ ,  $\log(M_{\text{H}}/M) = -4.50 \pm 0.02$  and the surface gravity derived from the model is  $\log(g) = 8.09$ . The effective temperature and the mass of the best-fit model determined from our asteroseismic analysis are in excellent agreement with the parameters derived from the GAIA precise photometry and parallax measurement:  $T_{\text{eff}} = 12259 \text{ K} \pm 68 \text{ K}$  and  $M/M_{\odot} = 0.631 \pm 0.005$  (Gentile Fusillo et al. 2019). From the rotational splitting we derived that GD 133 is rotating with a period of  $7.0 \pm 1.0$  days.

## ACKNOWLEDGEMENTS

We thank the referee, Dr. Pierre Bergeron, for his suggestions to improve the manuscript. J.-N.F. acknowledges the support from the National Natural Science Foundation of China (NSFC) through the grants 11673003 and 11833002. G.V. acknowledges financial support from "Programme National de Physique Stellaire" (PNPS) of CNRS/INSU, France and from Natural Science Foundation of China (NSFC) under the grant 11673003. J.S. acknowledges financial support from China Postdoctoral Science Foundation under the grant number 2015M570960 and support from Key Laboratory for the Structure and Evolution of Celestial Objects, Chinese Academy of Sciences, under the grant number OP201406. The data used in this paper were partially acquired using the RATIR instrument, funded by the University of California (UC) and NASA Goddard Space Flight Center (GSFC), on the 1.5 meter telescope at Observatorio Astronómico Nacional, San Pedro Mártir, operated and maintained by OAN-SPM and IA-UNAM. L.F.M. and R.M. acknowledge the financial support from the UNAM under grant PAPIIT IN100918.

Based on observations made with the 2.16-m and the

85 cm telescopes of Xinglong station operated by National Astronomical Observatories of Chinese Academy of Sciences (China), the 1.5 m and the 84 cm of the San Pedro Mártir observatory (Mexico), the 2.4 m telescope of Lijiang station operated by Yunnan Astronomical observatory of Chinese Academy of Sciences (China), the 1 m telescope of Nanshan station operated by Xinjiang Astronomical Observatory of Chinese Academy of Sciences (China), the 1 m telescope of Pic-du-Midi observatory (France) and the 1.8 m telescope of Bohyunsan Optical Astronomical Observatory (Korea).

## REFERENCES

- Bonsor A., Mustill A.J., Wyatt M.C., 2011, *MNRAS*, 414, 930  
Bradley P., 1993, PhD Thesis, University of Texas at Austin  
Breger M., Stich J., Garrido, R., et al. 1993, *A&A*, 271, 482  
Castanheira B.G. & Kepler S.O., 2008, *MNRAS*, 385, 430  
Croll B., Dalba P.A., Vandenburg A., et al. 2017, *ApJ*, 836, 82  
Deal M., Deheuvelds S., Vauclair G., et al. 2013, *A&A*, 557, L12  
Debes J.H. & Sigurdsson S., 2002, *ApJ*, 572, 556  
Debes J.H., Walsh K.J., Stark C., 2012, *ApJ*, 747, 148  
Farihi J., Jura M., Zuckerman B., 2009, *ApJ*, 694, 805  
Farihi J., Jura M., Lee J.-E., et al. 2010, *ApJ*, 714, 1386  
Frewen S.F.N. & Hansen B.M.S., 2014, *MNRAS*, 439, 2442  
Fu J.-N., Dolez N., Vauclair G., et al. 2013, *MNRAS*, 429, 1585  
Gänsicke B.T., Aungwerojwit A., Marsh T.R., et al. 2016, *ApJ*, 818, L7  
Gentile Fusillo N.P., Tremblay P.-E., Gänsicke B.T., et al. 2019, *MNRAS*, 482, 4570  
Gianninas A., Bergeron P., Ruiz M.T., 2011, *ApJ*, 743, 138  
Gizon L. & Solanki S.K., 2003, *ApJ*, 589, 1009  
Jura M., 2003, *ApJ*, 584, L91  
Jura M., 2008, *AJ*, 135, 1785  
Jura M., Farihi J., Zuckerman B., 2007, *ApJ*, 663, 1285  
Jura M., Farihi J., Zuckerman B., 2009, *AJ*, 137, 3191  
Kawka A., Vennes S., Dinnbier F., et al. 2011, *AIPC*, 1331, 238  
Kepler S. O., Giovannini O., Kanaan A., et al. 1995, *BaltA*, 4, 1571  
Koester D., Rollenhagen K., Napiwotzki R., et al. 2005, *A&A*, 432, 1025  
Koester D., Voss B., Napiwotzki R., et al. 2009, *A&A*, 505, 441  
Kuschnig R., Weiss W.W., Gruber R., et al. 1997, *A&A*, 328, 544  
Lajoie C.-P. & Bergeron P., 2007, *ApJ*, 667, 1126  
Lenz P. & Breger M., 2005, *CoAst*, 146, 53  
Li C., Fu J.-N., Vauclair G., et al. 2015, *MNRAS*, 449, 3360  
Montgomery M.H., 1998, PhD Thesis, University of Texas at Austin  
Mullally F., Winget D.E., Degennaro S., et al. 2008, *ApJ*, 676, 573  
Mukadam A.S., Bischoff-Kim, A., Fraser O., et al. 2013, *ApJ*, 771, 17  
Mustill A.J., Villaver E., Veras D., et al. 2013, *EPJWC*, 47, 06008  
Paxton B., Bildsten L., Dotter A., et al. 2011, *ApJS*, 192, 3  
Paxton B., Cantiello M., Arras P., et al. 2013, *ApJS*, 208, 4  
Paxton B., Marchant P., Schwab J., et al. 2015, *ApJS*, 220, 15  
Rappaport S., Gary B.L., Kaye T., et al. 2016, *MNRAS*, 458, 3904  
Romero A.D., Córscico A.H., Althaus L.G., et al. 2012, *MNRAS*, 420, 1462  
Sandhaus P.H., Debes J.H., Ely J., et al. 2016, *ApJ*, 823, 49  
Silvotti R., Pavlov M., Fontaine G., et al. 2006, *MmSAI*, 77, 486  
Su J. & Li Y., 2010, *RAA*, 10, 266  
Su J., Li Y., Fu J.-N., et al. 2014, *MNRAS*, 437, 2566  
Thoul A.A., Bahcall J.N., Loeb A., 1994, *ApJ*, 421, 828  
Vanderburg A., Johnson J.A., Rappaport S., et al. 2015, *Natur*, 526, 546  
Vauclair S., Vauclair G., Deal M., et al. 2015, *ASPC*, 493, 101  
Veras D., Wyatt M.C., Mustill A.J., et al. 2011, *MNRAS*, 417, 2104  
Veras D., Mustill A.J., Bonsor A., et al. 2013, *MNRAS*, 431, 1686  
Veras D., Leinhardt Z.M., Bonsor A., et al. 2014, *MNRAS*, 445, 2244  
Veras D., Jacobson S.A., Gänsicke B.T., 2014, *MNRAS*, 445, 2794  
Veras D., Eggl S., Gänsicke B.T., 2015a, *MNRAS*, 451, 2814  
Veras D., Leinhardt Z.M., Eggl S., et al. 2015, *MNRAS*, 451, 3453  
Veras D., Eggl S., Gänsicke B.T., 2015b, *MNRAS*, 452, 1945  
Veras D., 2016, *RSOS*, 3, 150571  
Veras D., Mustill A.J., Gänsicke B.T., et al. 2016, *MNRAS*, 458, 3942  
Wachlin F.C., Vauclair G., Vauclair S., et al. 2017, *A&A*, 601, 13  
Winget D.E., Cochran W.D., Endl M., et al. 2003, in *Scientific Frontiers in Research on Extrasolar Planets*, eds. D. Deling & S. Seager, ASP Conference Series, 294, 59  
Winget D.E., Hermes J.J., Mullally F., et al. 2015, in *19th European Workshop on White Dwarfs*, eds. P. Dufour, P. Bergeron & G. Fontaine, ASP Conference Series 493, 285  
Xu S., Jura M., Koester D., et al. 2014, *ApJ*, 783, 79  
Xu S., Jura M., Dufour P., et al. 2016, *ApJ*, 816, L22  
Zhang E.-H., Robinson E.L., Nather R.E., 1986, *ApJ*, 305, 740

This paper has been typeset from a  $\text{\TeX}/\text{\LaTeX}$  file prepared by the author.